Optical Nonlinearities of Fractal Composites

Vladimir M. Shalaev

School of Electrical and Computer Engeneering, Purdue University
West Lafayette, IN 47907-1285, USA
shalaev@purdue.edu

Abstract. A theory of optical responses in fractal nanostructured composite materials is outlined. It is shown that the fractal geometry results in localization of plasmon excitations in the "hot" spots, where the local field can exceed the applied field by several orders of magnitude. The high local fields of the localized fractal modes result in dramatic enhancement of optical responses, making surface-enhanced spectroscopy of single molecules and nanocrystals feasible.

1 Introduction

Electromagnetic phenomena in random metal–insulator composites, such as rough thin films, cermets, colloidal aggregates and others, have been intensively studied for the last two decades [1,2]. These media typically include small nanometer-scale particles or roughness features. Nanostructured composites possess fascinating electromagnetic properties, which differ greatly from those of ordinary bulk material, and they are likely to become ever more important with the miniaturization of electronic and optoelectronic components.

Giant enhancement of optical responses in a random medium including a metal component, such as metal nanocomposites and rough metal thin films consisting of small nanometer-sized particles or roughness features, is associated with optical excitation of surface plasmons that are collective electromagnetic modes and strongly depend on the geometric structure of the medium. Nanocomposites and rough thin films are often characterized by fractal geometry, where collective optical excitations, such as surface plasmons, tend to be localized in small nanometer-sized areas, namely, hot spots, because the plane running waves are not eigenfunctions of the operator of dilation symmetry that characterizes fractals.

Fractals look similar in different scales; in other words, a part of the object resembles the whole. Regardless of the size, this resemblance persists forever, if the object is mathematically defined. In nature, however, the scale-invariance range is restricted, on the one side, by the size of the structural units (e.g., atoms) and on the other, by the size of the object itself. The emergence of fractal geometry was a significant breakthrough in the description of irregularity [3]. The realization of the fact that the geometry of fractional dimensions is often more successful than Euclidean geometry in describing

V. M. Shalaev (Ed.): Optical Properties of Nanostructured Random Media,
Topics Appl. Phys. **82**, 93–112 (2002)

natural shapes and phenomena provided it a major impetus to research and led to better understanding of many processes in physics and other sciences.

Fractal objects do not possess translational invariance and therefore cannot transmit running waves [4]. Accordingly, dynamic excitations, such as, for example, vibrational modes (fractons), tend to be localized in fractals [4]. Formally, this is a consequence of the fact that plane running waves are not eigenfunctions of the operator of dilation symmetry characterizing fractals. The efficiency of fractal structures in damping running waves is probably the key to "self-stabilization" of many of the fractals found in nature [3].

The physical and geometric properties of fractal clusters has attracted growing attention from researchers in the past two decades [3,4]. The reason for this is twofold. First, processes of aggregation of small particles in many cases lead to the formation of fractal clusters rather than regular structures [3]. Examples include the aggregation of colloidal particles in solutions, the formation of fractal soot from little carbon spherules in the process of incomplete combustion of carbohydrates, the growth of self-affine films, and the gelation process and formation of porous media [3]. The second reason is that the properties of fractal clusters are very rich in physics and different from those of either bulk material or isolated particles (monomers) [2,4].

The most simple and extensively used model for fractal clusters is a collection of identical spherically symmetrical particles (monomers) that form a self-supporting geometric structure. It is convenient to think of monomers as identical rigid spheres that form a bond on contact. A cluster is considered self-supporting if each monomer is attached to the rest of the cluster by one or more bonds. Fractal clusters are classified as "geometric" (built as a result of a deterministic iteration process) or "random." Most clusters in nature are random.

The fractal (Hausdorff) dimension of a cluster D is determined through the relation between the number of particles N in a cluster (aggregate) and the cluster's radius of gyration R_c:

$$N = (R_c/R_0)^D \,, \tag{1}$$

where R_0 is a constant of the order of the minimum separation distance between monomers. Note that the fractal dimension is, in general, fractional and less than the dimension of the embedding space d, i.e., $D < d$. Such a power-law dependence of N on R_c implies a spatial scale-invariance (self-similarity) for the system. For the sake of brevity, we refer to fractal aggregates, or clusters, as fractals.

Another definition of the fractal dimension uses the pair density–density correlation function $\langle \rho(\mathbf{r})\rho(\mathbf{r}+\mathbf{R})\rangle$:

$$\langle \rho(\mathbf{r})\rho(\mathbf{r}+\mathbf{R})\rangle \propto R^{D-d}, \quad \text{if } R_0 \ll r \ll R_c \,. \tag{2}$$

This correlation makes fractals different from truly random systems, such as salt scattered on the top of a desk. Note that the correlation becomes

constant, $g(r) = \text{const}$, when $D = d$; this corresponds to conventional media, such as crystals, gases, and liquids. The unusual morphology of fractional dimensions results in unique physical properties of fractals, including the localization of dynamic excitations.

Optical excitations in fractal composites are substantially different from those in other media. For example, there is only one dipolar eigenstate that can be excited by a homogeneous field in a dielectric sphere (for a spheroid, there are three resonances with nonzero total dipole moment); the total dipole moment of all other eigenstates is zero and, therefore, they can be excited only by an inhomogeneous field. In contrast, fractal aggregates possess a variety of dipolar eigenmodes, distributed over a wide spectral range, which can be excited by a homogeneous field.

In continuous media, dipolar eigenstates (polaritons) are running plane waves that are eigenfuctions of the operator of translational symmetry. This also holds for most microscopically disordered media that are homogeneous on average. Dipolar excitations in these cases are typically delocalized over large areas, and all monomers absorb light energy at approximately the same rate in regions that significantly exceed the wavelength. In contrast, fractal composites have optical excitations that are localized in small subwavelength regions. The local fields in these "hot" spots are large, and the absorption by the "hot" monomers is much higher than by other monomers in a fractal composite. This is a consequence of the fact (mentioned above) that fractals do not possess translational symmetry; instead, they are symmetrical with respect to the scale transformation.

In metal fractal composites, the dipolar excitations are represented by plasmon oscillations. Plasmon modes are strongly affected by fractal morphology, leading to the existence of hot spots, which are areas of plasmon localization in fractals. Local enhancements in hot spots can exceed the average surface enhancement by many orders of magnitude because the local peaks of the enhancement are spatially separated by distances much larger than the peak sizes. The spatial distribution of these high-field regions is very sensitive to the frequency and polarization of the applied field [5]. The positions of the hot spots change chaotically but reproducibly with frequency and/or polarization. This is similar to speckles created by laser light scattered from a rough surface; the important difference is that the scale size for fractal plasmons in the hot spots is in the nanometer range rather than in the micrometer range encountered for photons.

The fractal plasmon, as any wave, is scattered from density fluctuations — in other words, fluctuations of polarization. The strongest scattering occurs from inhomogeneities of the same scale as the wavelength. In this case, interference in the process of multiple scattering results in Anderson localization. Anderson localization corresponds typically to uncorrelated disorder. A fractal structure is in some sense disordered, but it is also correlated for all length scales, from the size of constituent particles, in the lower limit, to the total size of the fractal, in the upper limit. Thus, what is unique for fractals is that, because of their scale invariance, there is no characteristic size of inhomogeneity — inhomogeneities of all sizes are present, from the lower to the upper limit. Therefore, whatever the plasmon wavelength, there are always fluctuations in a fractal with similar sizes, so that the plasmon is always strongly scattered and, consequently, can be localized [2,5].

Note that, as shown in [6], a pattern of localization of optical modes in fractals is complicated and can be called inhomogeneous. At any given frequency, individual eigenmodes are dramatically different from each other, and their sizes (their coherent radii) vary in a wide range, from the size of an individual particle to the size of a whole cluster. (In the vicinity of the plasmon resonance of individual particles, even chaotic behavior of the eigenmodes in fractals can be found [6].) However, even delocalized modes typically consist of two or more very sharp peaks that are topologically disconnected, i.e., located at relatively large distances from each other. In any case, the electromagnetic energy is mostly concentrated in these peaks, which can belong to different modes or, sometimes, to the same mode. Thus, despite the complex inhomogeneous pattern of localization in fractals, there are always very sharp peaks, where the local fields are high. These hot spots eventually provide significant enhancement for a number of optical processes, especially the nonlinear ones that are proportional to the local fields to a power greater than one.

Because of the random character of fractal surfaces, the high local fields associated with hot spots look like strong spatial fluctuations. Since a nonlinear optical process is proportional to the local fields raised to a power greater than one, the resulting enhancement associated with the fluctuation area (i.e., with the hot spot) can be extremely large. In a sense, we can say that enhancement of optical nonlinearities is especially large in fractals because of very strong field fluctuations.

Large fluctuations of local electromagnetic fields on the metal surfaces of inhomogeneous metal media result in a number of enhanced optical effects. A well known effect is surface-enhanced Raman scattering (SERS) by molecules adsorbed on a rough metal surface, e.g., in aggregated colloidal particles [7].

In an intense electromagnetic field, a dipole moment induced in a particle can be expanded into a power series: $d = \alpha^{(1)}E(r) + \alpha^{(2)}[E(r)]^2 + \alpha^{(3)}[E(r)]^3 + \ldots$, where $\alpha^{(1)}$ is the linear polarizability of a particle, $\alpha^{(2)}$ and $\alpha^{(3)}$ are the nonlinear polarizabilities, and $E(r)$ is the local field at site r. The polarization of a medium (i.e., dipole moment per unit volume), which is a source of the electromagnetic field in a medium, can be represented in an analogous form by the coefficients $\chi^{(n)}$ called "susceptibilities." When the local field exceeds the applied field, $E^{(0)}$, considerably, huge enhancements of nonlinear optical responses occur.

Below we first consider local-field enhancement in nanometer-sized metal particles and then the unique features of the enhancement that are opened up in fractal composites of metal nanoparticles.

2 Local-Field Enhancement in Nanospheres and Nanospheroids

Here we consider the local-field enhancement that can be obtained on the surfaces of individual metal nanoparticles, which are much smaller than the wavelength of the incident electromagnetic wave. In such particles, the excitation of free electrons (plasmons) can result in large local fields, much larger than the applied optical field. Plasmon oscillations (also referred to as surface plasmons) aare especially strong at the resonant excitation. This plasmon resonance is associated with collective electron oscillations (surface plasmons). The displacement of free electrons from their equilibrium position in a small particle results in a uncompensated charge on the surface of the particle, leading to its polarization; this polarization, in turn, results in a restoring force that causes electron oscillations. These plasmon oscillations can lead to the large local fields near the surface of the metal particle so that a molecule adsorbed on the metal surface can produce "surface-enhanced" optical signals. Possible shifts of molecular energy levels and creation of new resonances due, for example, to a charge transfer mechanism are not considered in this section; this enhancement (referred sometimes to as chemical enhancement) although important, is not universal and can occur only for special molecules. In contrast, electromagnetic enhancement is universal and takes place regardless of the possible "chemical" renormalization of the molecular cross section.

The metal particles we are concerned with are much smaller than the wavelength and have sizes in the range from 5 to 50 nm. The field enhancement, in this case, can be especially large. In bigger particles, the retardation effects that spoil the quality factor of the plasmon resonance become important; in smaller particles, electron scattering at the metal surface increases the resonance width and thus decreases the quality factor.

We note that since the plasmon resonance is due to the surface charge and thus is of a geometric nature, it depends only on the shape of a particle. For spheres, for example, with radii in the range roughly from 5 to 50 nm, the resonance frequency and its width almost do not depend on the particle's size.

The optical responses of metals can, in many cases, be well approximated with the Drude model. For a Drude metal, the dielectric constant is given by

$$\epsilon = \frac{4\pi \mathrm{i}\sigma}{\omega} = \epsilon_0 + \frac{4\pi \mathrm{i}\sigma(0)}{\omega[1 - \mathrm{i}\omega\tau]}\,, \tag{3}$$

where the dc conductivity $\sigma(0)$ is related to the plasma frequency ω_p and relaxation time τ by $\sigma(0) = \omega_\mathrm{p}^2\tau/(4\pi)$ and ϵ_0 is a contribution to ϵ due to interband electron transitions. (Note that for the relaxation rate of collective plasmon oscillations, $1/\tau$, the following different notations $1/\tau = \omega_\tau = \Gamma$ are interchangeably used in the literature and in this paper.) The Drude model describes well the optical response of free electrons in metals; through the term ϵ_0, it also takes into account the contribution to the dielectric constant due to interband electron transitions. The real and imaginary parts of the Drude dielectric function can also be represented as

$$\epsilon' = \epsilon_0 - \frac{\lambda^2}{\lambda_p^2}\frac{1}{1+(\lambda/\lambda_\tau)^2}, \qquad (4)$$

and

$$\epsilon'' = \frac{\lambda^3}{\lambda_p^2\lambda_\tau}\frac{1}{1+(\lambda/\lambda_\tau)^2}, \qquad (5)$$

where $\lambda/\lambda_\tau \equiv (\omega\tau)^{-1}$ and $\lambda/\lambda_p \equiv (\omega_p/\omega)$. For silver and gold, for example, $\lambda_\tau \sim 60\,\mu\mathrm{m}$ and $20\,\mu\mathrm{m}$, respectively, and $\lambda_p \sim 140\,\mathrm{nm}$.

Below, we consider spheroids, where two out of three semiaxes (a, b, and c) are equal: $b = c$. In a sphere, all of the semiaxes are the same, $a = b = c$. In prolate and oblate spheroids, $a > b = c$ and $a < b = c$, respectively. As is well known, the largest local fields can be obtained at the tip of sharp structures; therefore, we focus below on cigar-shaped spheroids, where $a \gg b$, and pancake-shaped spheroids, where $a \ll b$. We also assume that the field is polarized along the long axis of a spheroid, so that the largest field enhancement can be obtained. Then the polarizability of a spheroid can be written as

$$\alpha = \frac{V}{4\pi}\frac{\epsilon - 1}{1 + p(\epsilon - 1)}, \qquad (6)$$

where p is a depolarization factor, V is the volume of a nanospheroid, and the host medium was chosen, for simplicity, to be a vacuum. For a sphere, $p = 1/3$ and $V = (4\pi/3)R^3$, so that

$$\alpha_0 = R^3\frac{\epsilon - 1}{\epsilon + 2}, \qquad (7)$$

where R is the radius of the sphere. For prolate, cigar-shaped spheroids, $p \approx (b/a)^2[\ln(\sqrt{2}a/b) - 1]$. For all realistic aspect ratios $A = a/b$, the depolarization factor can be estimated as $p \sim (A)^{-2}$. [Really, for $A = 3$, $A = 10$, and $A = 100$, for example, $pA^2 \approx 0.4$, 1.6, and 4, respectively. It is also clear that A cannot be larger than 100 for particles that have a larger axis on a scale of 10 nm; in fact, since the quality factor decreases when any of the spheroid's axes is outside the range of 5–50 nm (see above), the aspect ratio for spheroids with high-quality resonance is limited roughly to 10.] For oblate, pancake-shaped spheroids, $p \approx (\pi/4)A^{-1}$, where the aspect ratio for oblate spheroids is defined as $A = b/a$. It is important to note that at the same aspect ratio A, the depolarization factor in the quasi-one-dimensional "cigars" (or needles) is much smaller than in quasi-two-dimensional pancakes (or disks). This fact has important consequences for field enhancement, as discussed below.

Now we consider the field enhancement that can be obtained in nano-sized spheres and spheroids. The largest field enhancement can be obtained at the plasmon resonance when the real part of the denominator in (6) becomes zero, i.e., at

$$\epsilon'_r \equiv \epsilon'(\lambda_r) = 1 - 1/p. \qquad (8)$$

According to the Drude model (4), the resonant frequency at $\lambda \ll \lambda_\tau$ is given by

$$\lambda_r = \lambda_p\,(1/p + \epsilon_0 - 1)^{1/2}. \qquad (9)$$

For a sphere, $\epsilon'_r = -2$; for spheroids with a large aspect ratio, $A \gg 1$, the depolarization factor is small, $p \ll 1$, so that $\epsilon'_r \approx -1/p$ and $\lambda_r \approx \lambda_p/\sqrt{p}$. The local-field enhancement E_l/E_0 at the surface of spheres and at the sharp edges of spheroids is estimated by the resonance quality factor Q_f as

$$\frac{E_l}{E_0} \sim Q_f \sim (4\pi/V)\alpha(\lambda_r), \qquad (10)$$

where $\alpha(\lambda_r)$ is the resonant value of the polarizability.

The local-field enhancement for a sphere is given by [see (7) and (10)]

$$Q_f \equiv Q_0 = \frac{|\epsilon'_r - 1|}{\epsilon''_r} = \frac{3}{(\epsilon_0 + 2)^{3/2}}\frac{\lambda_\tau}{\lambda_p} \sim \frac{\lambda_\tau}{\lambda_p}. \qquad (11)$$

For different noble metals, the magnitudes of Q_f are on the order of 10 to 100 (for silver, it is the largest, about 50 at the resonant frequency $\lambda_r \sim 400\,\mathrm{nm}$).

For a spheroid, according to (6) and (10), the resonant enhancement is estimated as

$$Q_f \sim \frac{1}{p}\frac{|\epsilon'_r|}{\epsilon''_r} \sim \frac{p^{-2}}{(p^{-1} + \epsilon_0 - 1)^{3/2}}\frac{\lambda_\tau}{\lambda_p} \sim \frac{\lambda_\tau}{\sqrt{p}\lambda_p}, \qquad (12)$$

where for the second estimate, we used (4), (5), and (9), and for the last estimate, we assumed that $1/p \gg \epsilon_0 - 1$. We note that the depolarization factor p is related to the resonance frequency via (9), so that (12) can also be written as

$$Q_f \sim \frac{(1 - \epsilon_0 + \lambda_r^2/\lambda_p^2)^2}{(\lambda_r/\lambda_p)^3}\frac{\lambda_\tau}{\lambda_p} \sim \frac{\lambda_r\lambda_\tau}{\lambda_p^2}, \qquad (13)$$

where for the last estimate, we assumed that $(\lambda_r/\lambda_p)^2 \gg \epsilon_0 - 1$.

According to (12), the local-field enhancement is estimated as

$$Q_f \sim A^2\frac{|\epsilon'_r|}{\epsilon''_r} \sim A\frac{\lambda_\tau}{\lambda_p} \sim AQ_0, \qquad (14)$$

for cigar-shaped spheroids, and as

$$Q_{\mathrm{f}} \sim A\frac{|\epsilon'_{\mathrm{r}}|}{\epsilon''_{\mathrm{r}}} \sim \sqrt{A}\frac{\lambda_{\mathrm{r}}}{\lambda_{\mathrm{p}}} \sim \sqrt{A}Q_0 \,, \tag{15}$$

for pancake-shaped spheroids.

One can see that the local-field enhancement in spheroids can significantly exceed that in spheres, especially, in cigar-shaped nanostructures, where it exceeds the quality factor in spheres roughly by the aspect ratio A. These larger values for field-enhancement in spheroids are achieved at the resonant frequencies, $\epsilon'(\lambda_{\mathrm{r}}) = 1 - 1/p$, which are significantly shifted toward the infrared part of the spectrum, where ϵ' is negative and large in magnitude so that the resonance can occur at very small values of the depolarization factor p.

Thus, to obtain strong field enhancement at a particular wavelength λ, one can use a nanospheroid with the aspect ratio such that $\epsilon'(\lambda) = -1/p+1 \approx -1/p$, for small p. However, it is not easy, in general, to fabricate a nanospheroid with a given aspect ratio. Besides, for spectroscopic purposes, we need to have enhancement in a broad spectral range, so that a spectroscopic signal from any optical transition of an arbitrary molecule can be enhanced.

An alternative possibility is to use structures formed by spherical nanoparticles (colloids, for example), which are typically much easier to make. For example, it is clear that a straight chain of N spheres should have roughly the same optical resonances as a prolate spheroid with the aspect ratio $A = N$. By taking different configurations of colloids, one can obtain resonances (and thus enhancement) at different optical frequencies that depend on the geometry of the whole structure. This approach, however, has the same drawback: there are only few frequencies at which the compact structure of nanospheres resonates because the dipole–dipole interactions between particles arranged in "conventional" geometry is long-range, so that a compact system of particles always resonates as a whole at the frequencies depending on the object's external surface. Really, if we integrate the dipole near-field, $\propto 1/r^3$, into the conventional $3d$ space, we obtain a logarithmic divergence; this indicates that the system resonates as a whole. For example, close-packed particles within a spherical volume have roughly the same optical response as the sphere within which the particles are packed, so that all of the resonances are grouped near λ_{r} such that $\epsilon'(\lambda_{\mathrm{r}}) = -2$.

Thus, in both spheroids and compact structures of colloidal particles, large enhancement can be achieved only at few frequencies depending on the geometry of the structure. For spectroscopic studies, however, it is very important to have a *broadband* enhancement. In other words, we would like to have the local-field enhancement as strong as in spheroids, but within a broad spectral range, including the visible and infrared parts of the spectrum, so that an optical signal from any molecular transition could be enhanced and probed spectroscopically.

In that sense, fractal nanostructures considered below seem to be t materials of choice. Because of the scale-invariant geometry of fractals, c tical excitations are not spread over the whole structure but rather tend be localized in small, nanometer-sized areas, which have very different lo geometries and thus resonate at different frequencies. As a result, fractals p vide enhancement within an unusually large spectral interval, from the ne UV to the far-infrared. Below, we consider two important classes of frac nanostructures, fractal aggregates of colloidal particles and metal–dielect films near the percolation threshold.

3 Local-Field Enhanced Optical Responses in Fractal Aggregates

Random fractal clusters are complex systems built from simple elementa blocks, e.g., particles, that are called monomers. It is important to emph size that the rich and complicated properties of fractal clusters are det mined by their global geometric structure rather than by the structure each monomer. In the formulation of a typical problem in the optics of fr tal clusters, the properties of monomers and the laws of physics for th interaction with the incident field and with each other are known, where the properties of a cluster as a whole must be found.

In Fig. 1, you see a picture of a typical fractal aggregate of colloidal s ver particles (obtained via an electron microscope). The fractal dimension these aggregates is $D \approx 1.78$. Using the well-known model of cluster–clust aggregation, colloidal aggregate can be readily simulated numerically [Note that voids are present on all scales, from the minimum (about the si of a single particle) to the maximum (about the size of the whole cluste this is an indication of the statistical self-similarity of a fractal cluster. T size of an individual particle is ~ 10 nm, whereas the size of the whole clust is ~ 1 µm.

The process of aggregation, resulting in clusters similar to that shown Fig. 1, can be described as follows. A large number of initially isolated a randomly distributed nanoparticles executes random walks in the solutio Encounters with other nanoparticles result in their sticking together; first form small groups, and then, in the course of the random walking, to agg gate into larger formations, and so on. Cluster–cluster aggregates (CCA with the fractal dimension $D \approx 1.78$, are thereby eventually formed.

When the constituent particles of a fractal cluster are irradiated by lig of amplitude $E^{(0)}$, oscillating dipole moments d_i are induced in them whi interact strongly through dipolar forces leading to the formation of collecti optical modes. (Note that throughout the text we interchangeably use t

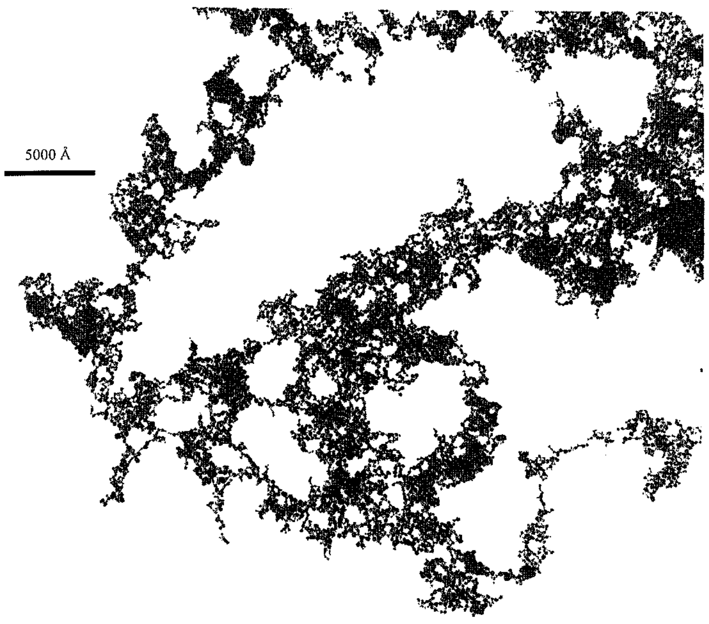

Fig. 1. Electron micrograph of a fractal colloid aggregate. Voids corresponding to all length scales are present; the minimum is the size of a single particle, the maximum is the size of the entire cluster. This is a graphic illustration of the statistical self-similarity and hence the fractal nature of the cluster. The radii of the individual particles is $\sim 10\,\mathrm{nm}$, and the size of the cluster is $\sim 1\,\mu\mathrm{m}$

notations E_0 and $E^{(0)}$ for the external field amplitude.) The coupled-dipole equations (CDE) for the induced dipoles acquire the following form [2]:

$$d_{i,\alpha} = \alpha_0 \left(E_\alpha^{(0)} + \sum_{j \neq i} W_{ij,\alpha\beta} d_{j,\beta} \right) . \tag{16}$$

In the quasi-static dipole approximation, for example, the interaction operator W between the dipoles has the form

$$W_{ij,\alpha\beta} = \langle \mathrm{i}\alpha | W | j\beta \rangle = \left(3 r_{ij,\alpha} r_{ij,\beta} - \delta_{\alpha\beta} r_{ij}^2 \right) / r_{ij}^5 , \tag{17}$$

where $\mathbf{r}_i$ is the radius vector of the ith monomer and $\mathbf{r}_{ij} = \mathbf{r}_i - \mathbf{r}_j$. The Greek indexes denote Cartesian components of vectors and should not be confused with the polarizability α_0 of spherical particles forming the aggregate.

Since $W_{ij,\alpha\beta}$ is independent of the frequency ω in the quasi-static approximation, the spectral dependence of solutions to (16) enters only through $\alpha_0(\omega)$. For convenience, we introduce the variable

$$Z(\omega) \equiv 1/\alpha_0(\omega) = -[X(\omega) + \mathrm{i}\delta(\omega)] . \tag{18}$$

Using (7), we obtain

$$X \equiv -\mathrm{Re}\left[\alpha_0^{-1}\right] = -R^{-3}\left[1 + 3(\epsilon' - 1)/|\epsilon - 1|^2\right] , \qquad (1$$

$$\delta \equiv -\mathrm{Im}\left[\alpha_0^{-1}\right] = 3R^{-3}\epsilon''/|\epsilon - 1|^2 . \qquad (2$$

The variable X indicates the proximity of ω to the resonance of an indivi ual particle, that occurs for a spherical particle at $\epsilon' = -2$ (that correspon to $X \approx 0$), and it plays the role of a frequency parameter; δ characteriz dielectric losses. The resonance quality factor is proportional to δ^{-1}. At t resonance of a spherical particle when $\epsilon' = -2$, $(R^3\delta)^{-1} = (3/2)|\epsilon'/\epsilon''|$. Ho ever, for the collective resonances of an ensemble of particles occurring $|\epsilon'| \gg 1$ (see below), $(R^3\delta)^{-1} \approx |\epsilon|^2/(3\epsilon'')$, which increases with the wav length. One can find $X(\lambda)$ and $\delta(\lambda)$ for any material using theoretical experimental data for $\epsilon(\lambda)$ and formulas (19), (20).

We can write (16) in matrix form. The Cartesian components of thre dimensional vectors $\mathbf{d}_i$ and $\mathbf{E}_{\mathrm{inc}}$ are given by $\langle i\alpha|d\rangle = d_{i,\alpha}$ and $\langle i\alpha|E_{\mathrm{inc}}\rangle$ $E_\alpha^{(0)}$. The last equality follows from the assumption that the incident fie is uniform throughout the sample. The matrix elements of the interactic operator are defined by $\langle i\alpha|\hat{W}|j\beta\rangle = W_{ij,\alpha\beta}$. Then (16) can be written a $[Z(\omega) - \hat{W}]|d\rangle = |E_{\mathrm{inc}}\rangle$. By diagonalizing the interaction matrix $\hat{W}$ wi $\hat{W}|n\rangle = w_n|n\rangle$ and expanding the $3N$-dimensional dipole vectors in terms the eigenvectors, we obtain the amplitudes of linear dipoles induced by t incident wave and the local fields. The local fields and dipoles are relat as [2] $E_{i,\alpha} = \alpha_0^{-1} d_{i,\alpha} = \alpha_0^{-1}\alpha_{i,\alpha\beta}E_\beta^{(0)}$. The local field E_{l} associated wi the ith particle, $E_{\mathrm{l}} = E_i$, can be found by solving the CDE as [2]

$$E_{i,\alpha} = \alpha_0^{-1} \sum_{j,n} \frac{\langle i\alpha|n\rangle\langle n|j\beta\rangle}{Z(\omega) - w_n} E_\beta^{(0)} . \qquad (2$$

Equation (21) allows one to express the local fields in terms of the eigenfun tions and eigenfrequencies of the interaction operator. The local fields c then be used to calculate the enhancement of various optical responses. No that this approach is not limited to a quasi-static approximation. Similar s lution can be obtained when the radiative terms in the interaction operat are taken into account [2].

When particles touch each other, the dipole approximation is not ad quate. The reason for this is that the dipole field ($\propto r^{-3}$ in the near zon generated by one monomer is not homogeneous inside the adjacent particl it is much stronger near the point where the monomers touch than in t center of the neighboring monomer. Effectively, by replacing two touchi spheres with two point dipoles located in their centers, we underestimate t actual strength of their interaction. To account for this effect, one typical has to take into account the higher multipolar terms.

Despite the fact that new efficient methods have recently been developed for calculations beyond the dipole approximation [8], they are still computationally applicable only for aggregates with relatively small number of particles or weak interactions between the particles. In aggregates of metal particles, where resonance plasmon oscillations can be excited and the dielectric constant can be very large, $|\epsilon'| \sim 10^3$ to 10^4, the interparticle interactions are very strong so that any direct computational calculations for aggregates of 10^4 particles are typically beyond the capability of any computer.

To overcome the inadequacy of the dipole approximation and the overwhelming computational load of the "coupled multipole" methods, a phenomenological procedure (that can be referred to as the cluster renormalization) approach has been suggested by Markel and Shalaev (see, for example, [2]). This method further develops the original idea suggested by Purcell and Pennypacker for odd-shaped objects and applies it to fractals. In this approach, a renormalized cluster is introduced in which neighboring spheres are allowed to intersect geometrically. This allows one effectively to take into account the stronger interaction between the neighboring particles, which, as mentioned, is undervalued by the "conventional" dipole approximation. The radii R of these spheres, as well as the distance a between two neighboring monomers, are chosen to be different from the real experimental ones: $R \neq R_{\text{exp}}$, $a \neq a_{\text{exp}}$, but it is required that the ratio a/R is equal to $(4\pi/3)^{1/3} \approx 1.612$, the same as in the Purcell and Pennypacker model (for details, see [2]). The second equation for R and a can be obtained from the optically important condition that the renormalized cluster has the same fractal dimension, radius of gyration, and total volume as the experimental cluster. It was shown that for fractals, where $D < 3$, all of these conditions are compatible, in contrast to nonfractal clusters of particles. The above model of effective intersecting particles allows one to take into account the stronger depolarization factors for touching particles, remaining within the "renormalized" dipole approximation. The model, it was shown, yields results that are in very good agreement with experimental spectra of fractal clusters [2].

Figure 2 shows the local field E_i distribution excited by light of wavelength $\lambda = 1\,\mu\text{m}$ at the surface of a simulated silver CCA deposited on a plane substrate. This distribution was computed by using solution (21) and the renormalized dipole approximation described above. The largest fields are extremely localized; the local field intensity in the "hot" spots can exceed the applied field by up to 10^5, and the average enhancement is only $\sim 10^2$ to 10^3.

The resonance local field is estimated by $|E_r/E^{(0)}| \sim 1/\delta$, as follows from (21), which is the exact solution (for simplicity, hereafter we set $R = 1$). This result can also be obtained from the simple fact that the linear polarizability $\alpha_i = d_i/E^{(0)}$ of the ith monomer in a cluster experiences a shift of resonance w_i because of interactions with other particles (where w_i is a real number, in the quasi-static approximation). Therefore, the polarizability of, say, the ith particle can always be represented as $\alpha_i = 1/(\alpha_0^{-1} + w_i) = [(w_i - X) - i\delta]^{-1}$, where the shift w_i depends on interactions with all particles. In the limit of noninteracting particles, $w_i = 0$ and $\alpha_i = \alpha_0 = -(X + i\delta)^{-1}$. For resonance particles, $w_i = X(\omega_r) \equiv X_r$, and $\alpha_r = i/\delta$. The local field is related to the local polarizability as $E_i = \alpha_0^{-1}\alpha_i E^{(0)}$, so that for $X \gg \delta$, we obtain $|E_r| \sim (|X_r|/\delta)|E^{(0)}|$ for the resonance field. In the optical spectral range, $|X_r| \sim 1$, and $|E_r| \sim \delta^{-1}|E^{(0)}|$. This estimate agrees qualitatively with the results shown in Fig. 2.

In the long wavelength part of the spectrum, where $|\epsilon'| \gg 1$, we see that $E_r/E^{(0)} \sim \delta^{-1} \sim |\epsilon'|^2/\epsilon''$. To compare with cigar-shaped spheroids, where $|\epsilon'_r| \sim 1/p \sim A^2$, we can write the enhancement in fractals formally as $E_r/E^{(0)} \sim p^{-1}|\epsilon'_r|/\epsilon''_r \sim A^2|\epsilon'_r|/\epsilon''_r \sim A(\lambda_\tau/\lambda_p)$. Since $A \sim |\epsilon'|^{1/2} \sim (\lambda/\lambda_p)$, the local field enhancement in fractals increases with λ as $E_r/E^{(0)} \sim (\lambda\lambda_\tau)/\lambda_p^2$. Thus, a fractal, with its variety of local configurations of particles (where optical excitations are localized), can be roughly thought of as a collection of (noninteracting) prolate nanospheroids, with all possible values of the aspect ratio.

It is worth noting again that if a fractal structure is replaced by some $3d$ compact structure of spheroids (or any other particles), then, because of the long-range interactions in nonfractal systems, there would, in general, be no localization of the optical excitations in such a structure. Instead, in most normal modes, every particle contributes significantly to the excitation, so that all the resonances depend on the shape of the whole object and lie typically within a relatively narrow spectral interval.

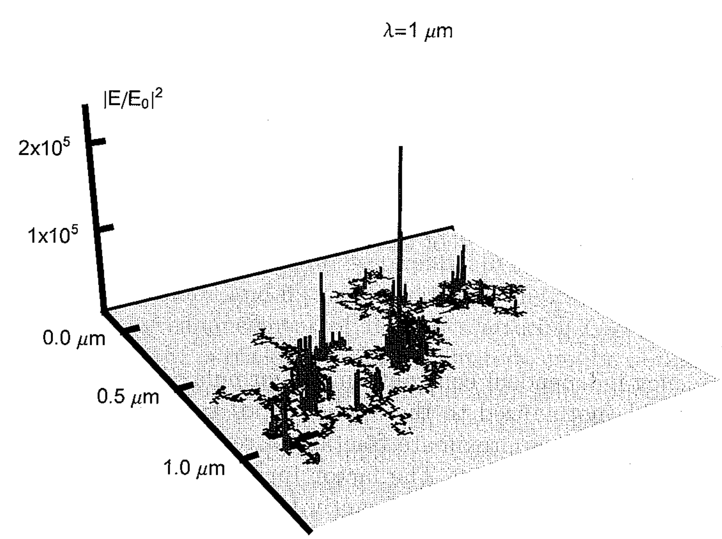

Fig. 2. Calculated field distributions on the surface of a silver fractal aggregate deposited on the plane

In fractals, in contrast, the resonance frequency of a localized surface plasmon mode depends on the local configuration of particles at the mode location. A random fractal is composed of a large variety of local geometries, each possessing a different plasmon resonance frequency; as a result, the range of frequencies spanned by the plasmon modes in a fractal cluster is unusually broad, covering the whole of the visible and infrared portions of the spectrum. Additionally, for most metals, the electromagnetic energy and the enhancement of nonlinear optical effects and Raman scattering increase toward longer wavelengths [2] because for most metals, the real part of the dielectric function is negative (that is why metals are such good reflectors) and its magnitude increases strongly toward longer wavelengths, resulting in a parallel increase in the quality factor of the plasmon resonances of fractal clusters composed of metal particles.

Locally intense fields, as shown in Fig. 2, suggest a large number of unusual local optical and photochemical effects, among them, single-molecule spectroscopy. Specifically, because the local enhancement-factor $\propto |E|^4$ [7] for surface-enhanced Raman scattering (SERS), it can reach magnitudes of 10^{12}, making Raman spectroscopy of single molecules possible [9].

4 Enhanced Optical Nonlinearities in Fractals

The local-field enhancement for a nonlinear optical process can, in general, be written as

$$G_n \sim \langle |E_i/E^{(0)}|^k [E_m/E^{(0)}]^m \rangle \,, \tag{22}$$

where $n = k+m$. In particular, $k = 4$, $m = 0$ describes the field enhancement for SERS, and $k = 2$, $m = 2$ for nonlinear refraction (the optical Kerr effect). Signals associated with coherent nonlinear light scattering, such as four-wave mixing (FWM), are proportional to the average square of the nonlinear polarization; hence the FWM enhancement, for example, is [2] $G_{\mathrm{FWM}} = |G_4|^2$.

For fractals, an estimate for G_n (at $k \neq 0$) can be expressed in terms of the polarizability $\alpha_0 \equiv -[X(\omega) + i\delta(\omega)]^{-1}$ of the individual particles composing the fractal as [2]

$$G_n \sim c_n |X|^n \delta^{1-n} \mathrm{Im}\,[\alpha(X)] \,, \tag{23}$$

where c_n is a frequency-independent constant. In this formula, $(|X|/\delta)^n$ gives the resonant local field (normalized to the applied field) raised to the nth power, and $\delta \mathrm{Im}\,[\alpha(X)]$ is the approximate fraction of resonant particles in the fractal for a given light frequency. The factor $\mathrm{Im}\,[\alpha(X)]$ represents the average light extinction, which differs significantly for fractals ($D < d$) and nonfractals ($D = d$).

For the average local-field intensity ($n = 2$), it can be shown that the *exact* result is given by

$$G = G_2 = \frac{(X^2 + \delta^2)}{\delta} \mathrm{Im}\,[\alpha(X)] \,, \tag{24}$$

in agreement with the estimate (23).

It is worth noting here that zero-point field fluctuations, which are responsible for spontaneous emission, are expected to be enhanced in the same manner as their "classical" counterparts, so that formula (24) also characterizes the enhancement of spontaneous emission in fractals.

For nonfractal random systems, the extinction $\mathrm{Im}\,[\alpha(X)]$ typically peaks near the resonance frequency of the individual particles (where $X(\omega) \approx 0$), becoming negligible for $|X| \gg \delta$, so that G_n, according to (23), is relatively small [2]. Contrariwise, for fractals, the factor $\mathrm{Im}\,[\alpha(X)]$ remains significant even in the long wavelength part of the spectrum, where $|X(\omega)| \gg \delta$, leading to very large values of G_n [2] ($\mathrm{Im}\,\alpha(X)$ has roughly a box-like distribution in the interval $-4\pi/3 \leq X \leq 4\pi/3$, which in terms of λ includes the whole of the visible and infrared parts of the spectrum [2]). Thus, the large enhancement in a broad spectral range, as mentioned, is a direct result of the localization of optical excitations and of the broad variety of resonating local structures.

We also note here that by exciting all (or most of) the fractal modes and matching their phases, one can produce attosecond light pulses because the extremely large spectral range of fractal modes (from the near-UV to the far-IR) in the spectral domain corresponds to attosecond time intervals in time domains.

For example, for Raman scattering with a small Stokes shift, the enhancement is given by $G_{\mathrm{RS}} \sim \langle |E|^4 \rangle / |E_0|^4$ [7] so that the above estimate in this case is as follows:

$$G_{\mathrm{RS}} \sim C_{\mathrm{RS}} X^4 \delta^{-3} \mathrm{Im}\,[\alpha(X)] \,, \tag{25}$$

where C_{RS} is a constant prefactor.

In Fig. 3a, we compare this analytical formula with the results of numerical solution for the CDEs for fractal aggregates with $D = 1.78$ (two different values for parameters δ are used). One can see that the theoretical formula is in good accord with numerical simulations. As seen in Fig. 3a, the product $G_{\mathrm{RS}}\delta^3$ does not depend systematically on δ in the important region close to the maximum, and its value there is of an order of one. Thus, we conclude that strong enhancement of Raman scattering $G_{\mathrm{RS}} \sim \delta^{-3}$, resulting from aggregation of particles into fractal clusters, can be obtained.

In Fig. 3b, surface-enhanced RS data obtained for colloidal silver solutions in experiments [7] is compared with the G_{RS} calculated with the use of (25). [The values of X and δ at different λ were found using formulas (19), (20)]. Note that only the spectral dependence of G_{RS} is informative in this figure since only relative values of G_{RS} were measured in [7]. The experimental data presented in Fig. 3b are normalized by setting $G_{\mathrm{RS}} = 28\,250$ at 570 nm, which is a reasonable value. Clearly, the present theory successfully explains the huge enhancement accompanying aggregation of particles into fractals

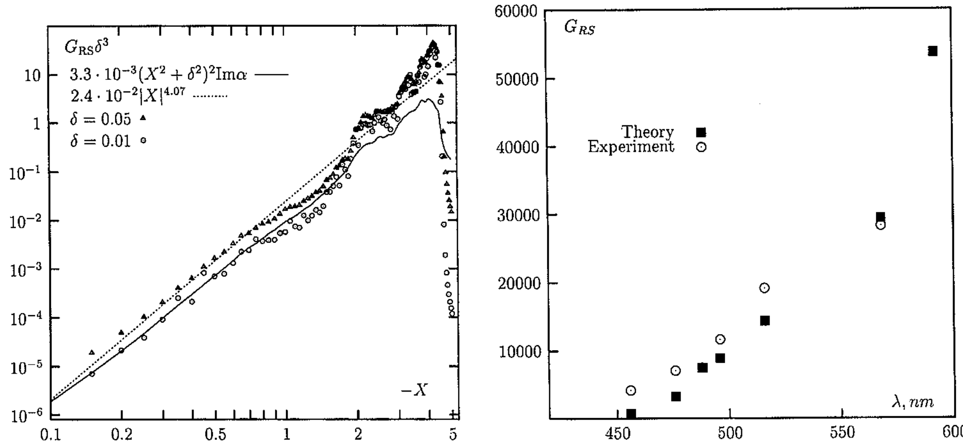

Fig. 3. (**a**) Enhancement of Raman scattering in cluster–cluster aggregates (CCAs) (multiplied by δ^3) for negative X, corresponding to the visible and infrared parts of the spectrum. (**b**) Theoretical and experimental enhancement factors for Raman scattering in colloidal silver aggregates as functions of wavelength λ

and the observed increase of G_{RS} toward the red part of the spectrum. The strong enhancement toward the red occurs because the local fields associated with collective dipolar modes in CCAs become significantly larger in this part of the spectrum.

We note that the same enhancement characterizes Kerr optical nonlinearity, which is responsible for nonlinear refraction and absorption, $G_K \sim \langle |E|^2 E^2 \rangle / |E_0|^2 E_0^2 \sim G_{\mathrm{RS}}$ [2].

For coherent processes, the resultant enhancement $\sim |\langle |E_i/E^{(0)}|^n \rangle|^2$. For quasi-degenerate four wave-mixing (FWM), additional enhancement of the generated nonlinear amplitudes oscillating at almost the same frequency as the applied field should also be included, so that is given by $G_{\mathrm{FWM}} \sim |\langle |E|^2 E^2 \rangle|^2 / |E_0|^8$. We can estimate the FWM enhancement factor, $G_{\mathrm{FWM}} \sim |G_K|^2$, as [2]

$$G_{\mathrm{FWM}} \sim C_{\mathrm{FWM}} X^8 \delta^{-6} \left\{ \mathrm{Im}\left[\alpha(X)\right] \right\}^2 . \qquad (26)$$

All of these estimates agree with the results of analytical and numerical calculations [2].

Figure 4 shows the results of numerical calculations of the enhancement factor G_{FWM} in silver CCAs as a function (a) of spectral parameter X and as a function (b) of wavelength λ. The simulations were performed by solving the CDEs, and the simulation results were compared with the above analytical formula. The solid lines in Fig. 4a,b describe the results of calculations based on formula (26), with C_{FWM} found from the relation $G_{\mathrm{FWM}}\delta^6 = 1$; its maxima occur at $X \approx \pm 4$. The dashed line in Fig. 4a represents a power-law fit for the range $0.1 \le |X| \le 3$, with $\delta = 0.05$. The computed exponent

(8.31 ± 1.00) is close to 8 (only the negative values of X are shown; the results for positive X are qualitatively similar).

We conclude that formula (26) is in good agreement with numerical simulations in a wide range from the visible to the mid-infrared. Note that for $\lambda > 10\,\mu\mathrm{m}$, the resonance condition $\lambda \ll \lambda_\tau$ does not hold, and therefore the theory, strictly speaking, cannot be applied (for silver, $\omega_\tau \equiv \Gamma \approx 0.021\,\mathrm{eV}$, i.e., $\lambda_\tau \approx 56\,\mu\mathrm{m}$).

As seen in Fig. 4a,b, the enhancement strongly increases toward larger values of $|X|$ (when $X < 0$) or, in other words, toward longer wavelengths, where enhancements for the local fields are stronger.

It also follows from Fig. 4a that the product $G_{\mathrm{FWM}}\delta^6$ remains, on average, the same for the two very different values of δ chosen, namely, 0.01 and 0.05. This indicates that, in accordance with (26), the enhancement is proportional to the sixth power of the resonance quality factor, i.e., $G_{\mathrm{FWM}} \propto Q^6$ ($Q \sim \delta^{-1}$) and reaches huge values in the long-wavelength part of the spectrum where $X \approx X_0 = -4\pi/3$.

The nonlinear susceptibility $\bar{\chi}^{(3)}$ of a composite material, consisting of fractal aggregates of colloidal particles in some host medium (e.g., water) is given by $\bar{\chi}^{(3)} = p \cdot G_K \chi_m^{(3)}$ where $G_K \sim G_{\mathrm{FWM}}^{1/2}$ is the enhancement of the Kerr optical nonlinearity, $\chi_m^{(3)}$ is the susceptibility of nonaggregated metal particles, and p is the volume fraction filled by metal.

When the initially separated silver particles aggregate and fractal clusters are formed, a huge enhancement of the cubic susceptibility can occur. A millionfold enhancement of degenerate FWM (DFWM) due to the clustering of initially isolated silver particles in colloidal solution was experimentally obtained [10]. The observed enhancement factor for fractal silver composites

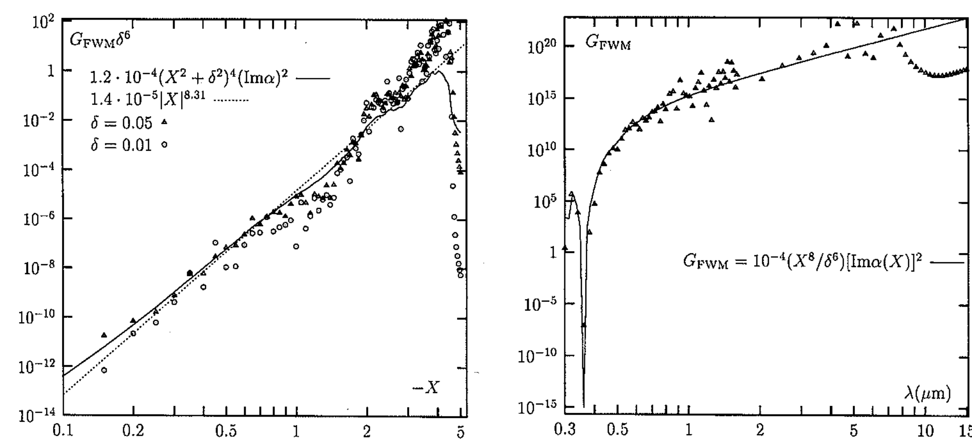

Fig. 4. Calculated enhancement for degenerate four-wave mixing, G_{FWM}. (**a**) $G_{\mathrm{FWM}}\delta^6$ as a function of X ($X < 0$) for CCAs; (**b**) G_{FWM} as a function of wavelength for silver CCAs

in these experiments is $G \sim 10^6$ for $\lambda = 532$ nm. Note that in Fig. 4b calculations are done with vacuum as a host medium, whereas the experiments were performed in an agueous colloidal solution. The values of X and δ for silver particles in water at laser wavelength $\lambda = 532$ nm are $X \approx -2.55$ and $\delta \approx 0.05$, respectively. According to Fig. 4a, $G_{\mathrm{FWM}} \sim 10^6$ to 10^7 for these values of X and δ, which is in reasonable agreement with the experimental observations.

The cubic susceptibility obtained experimentally for an aggregated sample is [10]: $|\bar{\chi}^{(3)}| = 5.7 \times 10^{-10}$ esu with $p \approx 5 \times 10^{-6}$. Note that p is a variable quantity and can be increased. We can assign the value 10^{-4} esu to the nonlinear susceptibility, $\chi^{(3f)}$, of the fractal clusters, i.e., $\bar{\chi}^{(3)} = p \cdot \chi^{(3f)}$, with $\chi^{(3f)} \sim 10^{-4}$ esu. This is a very large value for a third-order nonlinear susceptibility.

When characterizing potential applications of materials, it is important to have large $\chi^{(3)}$ at a relatively small absorption. As a characteristic of the materials, the figure of merit F can be used that is defined via the ratio of the nonlinear susceptibility $\bar{\chi}^{(3)}$ of a composite material and its linear losses that are given by the imaginary part of the effective (linear) dielectric function, $\bar{\epsilon}'' = 4\pi \mathrm{Im}\,[\bar{\chi}^{(1)}]$. Thus, the figure of merit is defined through the relation $|\bar{\chi}^{(3)}/\bar{\epsilon}''| = F\chi_0^{(3)}$, where $\chi_0^{(3)}$ is a "seed" optical nonlinearity that can be due either to particles forming the composite (then, $\chi_0^{(3)} = \chi_m^{(3)}$) or due to some nonlinear adsorbant molecules (we assume that the former is the case). Results of calculations of F for fractal silver aggregates (CCAs) are shown in Fig. 5, as a function of wavelength (nm). It can be seen that the figure of merit in the fractals is very large, $\sim 10^7$, in the near-infrared part of the spectrum where absorption is relatively small, whereas enhancement of optical nonlinearities is very significant.

A large variety of optical processes can be enhanced and otherwise modified by incorporating fractal clusters in the media or by ensuring that aggregation results in fractals. For example, fractals can be used to improve the performance of random lasers, such as powder lasers, and laser paints [11], where lasing emissions can take place as a result of coherent multiple light-scattering in a disordered dielectric (or semiconductor) with appropriate structural elements. The notion of creating a "ring" laser cavity in a random medium through a sequence of multiple coherent scattering events along a closed path is itself, a fascinating, and almost counterintuitive prospect. Scattering is normally considered detrimental to lasing since, in a conventional laser cavity, it tends to remove photons from the lasing mode. In a properly constructed random medium, however, strong multiple scattering could return photons to the amplification region resulting in mode amplification [11]. By doping the laser powder or paint medium with fractal aggregates or by imparting a fractal character to the medium as a whole, one could significantly decrease the pump power needed to effect lasing, in other words, one could decrease the lasing threshold.

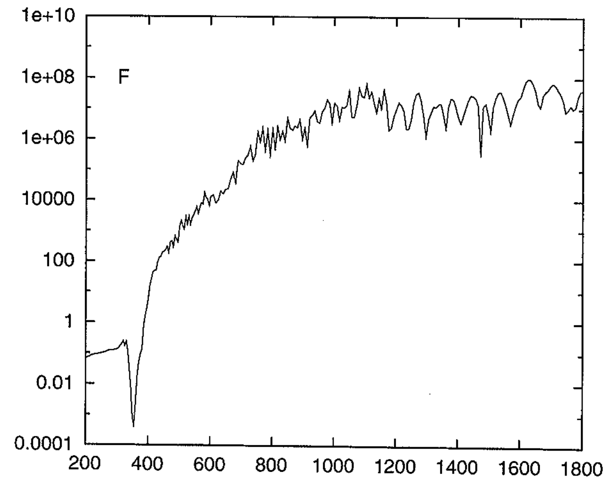

Fig. 5. The figure of merit F for fractal silver CCAs; F is the ratio of nonlinear susceptibility $|\bar{\chi}^{(3)}|$ and linear losses $\bar{\epsilon}''$ (see text). The wavelength λ is given in nanometers

As discussed in a separate contribution of this book, even more gigantic enhancement can be obtained by combining (multiplicatively) the local-field enhancement in fractals with the enhancement occurring in microcavities [2,12]. In these novel composite materials, microcavities doped with fractals, record-high enhancement of optical phenomena can be obtained.

Acknowledgements

This work was supported in part by National Science Foundation under Grant No. DMR-0121814, Army Research Office under Grant No. DAAD19-01-1-0682, Petroleum Research Fund, and NASA under Grants No. NAG 8-1710 and NCC-1-01049.

References

1. J. C. Garland, D. B. Tanner (Eds.), *Electron Transport and Optical Properties of Inhomogeneous Media* (AIP, New York 1978); W. L. Mochan, R. G. Barrera (Eds.), *Electron Transport and Optical Properties of Inhomogeneous Media (ETOPIM 3)* (North-Holland, Amsterdam 1994); A. M. Dykhne, A. N. Lagarkov, A. K. Sarychev. (Eds.), Physica A **241**, (1–2), 1 (1997), Proceedings (ETOPIM 4)
2. V. M. Shalaev, *Nonlinear Optics Of Random Media: Fractal Composites and Metal-Dielectric Films*, Springer Tracts in Modern Physics **158** (Springer, Berlin, Heidelberg 2000)
3. B. B. Mandelbrot, *The Fractal Geometry of Nature* (Freeman, San Francisco 1982); B. Sapoval, *Fractals* (Aditech, Paris 1990); A. L. Barbasi, H. E. Stanley,

Fractal Concepts in Surface Growth (Cambridge University Press, Cambridge 1995); R. Jullien, R. Botet, *Aggregation and Fractal Aggregates* (World Scientific, Singapore 1987)
4. S. Alexander, R. Orbach, J. Phys. Lett. **43**, 625 (1982); A. Bunde, S. Havlin (Eds.), *Fractals and Disordered Systems* (Springer, Berlin, Heidelberg 1991); L. Pietroniero, E. Tosatti (Eds.), *Fractals in Physics* (North-Holland, Amsterdam 1986); B. Sapoval, Th. Gorbon, A. Margolina, Phys. Rev. Lett. **67**, 2974 (1991)
5. V. M. Shalaev, M. I. Stockman, Sov. Phys. JETP **65**, 287 (1987); A. V. Butenko, V. M. Shalaev, M. I. Stockman, Z. Phys. D **10**, 81 (1988); V. A. Markel, L. S. Muratov, M. I. Stockman, T. F. George, Phys. Rev. B **43**, 8183 (1991); M. I. Stockman, L. N. Daudey, L. S. Muratov, T. F. George, Phys. Rev. Lett. **72**, 2486 (1994); D. P. Tsai, J. Kovacs, Z. Wang, M. Moskovits, V. M. Shalaev, J. S. Suh, R. Botet, Phys. Rev. Lett. **72**, 4149 (1994); V. M. Shalaev et al., Phys. Rev. B **53**, 2437 (1996); Ibid. **53**, 2425 (1996); V. M. Shalaev, Phys. Rep. **272**, 61 (1996); V. P. Safonov et al., Phys. Rev. Lett. **80**, 1102 (1998)
6. M. I. Stockman, L. N. Pandey, T. F. George, Phys. Rev. B **53**, 2183 (1996); M. I. Stockman, Phys. Rev. E **56**, 6494 (1997); Phys. Rev. Lett. **79**, 4562 (1997)
7. M. Moskovits, Rev. Mod. Phys. **57** , 783 (1985); R. K. Chang, T. E. Furtak (Eds.), *Surface Enhance Raman Scattering*, (Plenum, New York 1982); M. I. Stockman, V. M. Shalaev, M. Moskovits, R. Botet, T. F. George, Phys. Rev. B **46**, 2821 (1992)
8. J. B. Pendry, A. MacKinnon, Phys. Rev. Lett. **69**, 2772 (1992); F. J. Garcia-Vidal, J. M. Pitarke, J. B. Pendry, Phys. Rev. Lett. **78**, 4289 (1997); F. J. Garcia de Abajo, Phys. Rev. Lett. **82**, 2776 (1999)
9. K. Kneipp, Y. Wang, H. Kneipp, L. T. Perelman, I. Itzkan, R. D. Dasari, M. Feld, Phys. Rev. Lett. **78**, 1667 (1997); S. Nie, S. R. Emory, Science **275**, 1102 (1997)
10. S. G. Rautian, V. P. Safonov, P. A. Chubakov, V. M. Shalaev, M. I. Stockman, JETP Lett. **47**, 243 (1988) [transl. from Pis'ma Zh. Eksp. Teor. Fiz. **47**, 200 (1988)]; Yu. E. Danilova, V. P. Drachev, S. V. Perminov, V. P. Safonov, Bull. Russian Acad. Sci. Phys. **60**, 342 (1996); ibid., 374; Yu. E. Danilova, N. N. Lepeshkin, S. G. Rautian, V. P. Safonov, Physica A **241**, 231 (1997); F. A. Zhuravlev, N. A. Orlova, V. V. Shelkovnikov, A. I. Plehanov, S. G. Rautian, V. P. Safonov, JETP Lett. **56**, 260 (1992)
11. V. S. Letokhov, Soviet Phys. JETP **26**, 835 (1968); N. M. Lawandy et al., Nature **368**, 436 (1994); D. S. Wiersma, A. Lagendijk, Phys. Rev. E **54**, 4256 (1996); S. John, G. Pang, Phys. Rev. A **54**, 3642 (1996); G. A. Berger, M. Kempe, A. Z. Genack, Phys. Rev. E **56**, 6118 (1997); H. Cao et al. Phys. Rev. Lett. **82**, 2278 (1999); Phys. Rev. B **61**, 1985 (2000)
12. W. Kim, V. P. Safonov, V. M. Shalaev, R. L. Armstrong, Phys. Rev. Lett. **82**, 4811 (1999); V. P. Drachev, W. Kim, V. P. Safonov, V. A. Podolskiy, N. S. Zakovryazhin, V. M. Shalaev, R. A. Armstrong, J. Mod. Opt., in press (2001); V. A. Podoskiy, V. M. Shalaev, Laser Phys. **11**, 26 (2000)

Nonlinear Optical Effects and Selective Photomodification of Colloidal Silver Aggregates

Vladimir P. Drachev[1], Sergey V. Perminov[1], Sergey G. Rautian[2], and Vladimir P. Safonov[2]

[1] Institute of Semiconductor Physics, Siberian Branch of the Russian Academy of Sciences, Novosibirsk 630090, Russia
vdrachev@yahoo.com
[2] Institute of Automation and Electrometry, Siberian Branch of the Russian Academy of Sciences, Novosibirsk 630090, Russia

Abstract. Colloidal silver aggregates of nanoparticles were studied experimentally using optical spectroscopy, electron microscopy, near-field optics, and nonlinear optics. Changes in absorption spectra, local structure, and near-field optical response after the irradiation of fractal colloidal aggregates with a laser pulse (selective photomodification) were studied. The diameters of the selectively photomodified domains decreased as the laser wavelength increased, in accordance with the theory of the optics of fractal clusters. Giant enhancements of nonlinear optical responses were found for aggregated nanocomposites compared with nonaggregated. The enhancements are due to excitation of the collective plasmon modes in the aggregates. The plasmon modes are anisotropic and chiral. Nonlinear effects governed by local and nonlocal responses (degenerate four-wave mixing, nonlinear absorption, refraction and gyrotropy, inverse Faraday effect, and ellipse self-rotation) were studied.

The optics of aggregated metal–dielectric composites attracted considerable attention during the last two decades. This attention was due to increasing interest in the physics of the cooperative interaction of particles in random structures and the high application potential of metal nanostructures as nonlinear media, as substances, strongly facilitated to microanalysis, and media for optical data storage. Surface-enhanced Raman scattering [1], enhanced optical nonlinearities from local [2,3,4] and nonlocal [5] response, and selective photomodification of colloidal silver aggregates [6,7] have been studied. The effect of giant fluctuations of local electrical fields in colloidal aggregates, predicted in [8], were demonstrated in these experiments. Together with this, the experiments [3,6] facilitated the development of new techniques for investigating optical processes in aggregated metal nanocomposites.

Traditionally, an essential part of the data regarding the optics of new materials is gained by studying spectra of linear light absorption and scattering. An analysis of linear absorption spectra of metal nanoparticles and small aggregates is given in detail in [9]. The optical properties of a single metal nanosphere are governed to a large extent by excitation of the

V. M. Shalaev (Ed.): Optical Properties of Nanostructured Random Media, Topics Appl. Phys. **82**, 113–147 (2002)